Observational Evidence Of Effects Of Absorbing Aerosols On Seasonal–to– Interannual Anomalies Of The Asian Monsoon

K.–M. Lau, K.–M. Kim and N.–C. Hsu
Laboratory for Atmospheres, NASA/Goddard Space Flight Center, USA
Corresponding author: lau@climate.gsfc.nasa.gov

Absorbing aerosols, such as dust and black carbon, are characterized by their ability to heat the atmosphere by absorbing solar radiation. In contrast, non-absorbing aerosols such as sulfate, scatter solar radiation and have relatively small atmospheric heating effect. Yet, both absorbing and non-absorbing aerosols cause surface cooling by blocking solar radiation from reaching the earth's surface. This has been referred to as the "global dimming" effect (Stanhill and Cohen 2001). The dimming effect is global, even though sources of aerosols are local, because of the abundance and diverse geographic locations of the sources, continuous emission, and long-range transport of aerosols. In recent coupled model experiments, Ramanathan et al (2005) show that as a result of "global dimming", the Indian monsoon is reduced on decadal or longer time scales. From atmospheric GCM experiments, Menon et al (2002) showed that heating by increasing atmospheric loading of black carbon in the Asian monsoon region may be responsible for the long-term drought pattern over northern China. More recently, Lau et al (2005) point out that, on intraseasonal to interannual time scales, heating by absorbing aerosols may induce a tropospheric temperature anomaly over the northern India and Tibetan regions in late spring and early summer, subsequently leading to an earlier onset and intensification of the Indian monsoon. They propose the importance of the "elevated heat pump" effect of atmospheric heating by dust transported from the nearby deserts to northern India, stacking up against the southern slopes of the Himalayas. The dust combined with the black carbon from industrial and agricultural pollution in northern India provide an anomalous diabatic heat source, which triggers positive feedback in monsoon convective heating, enhancing the Indian monsoon. These results suggest that aerosol effects on monsoon water cycle dynamics are complex and likely to be a strong function of spatial and temporal scales.

Up to now, there has been no convincing observational evidence of aerosol effects on monsoon climate variability because of the lack of long-term (> 10 years) aerosol data. Recent satellite observations such as MODIS, MISR from NASA EOS have provided much needed, but still inadequate information on aerosol radiative properties. Since aerosol-induced anomalies are likely to be further confounded by the strong influence of a variety of forcing agents, including El Niño, Indian Ocean and West Pacific sea surface temperature anomalies, and possibly from global warming, the lack of reliable, long-term aerosol data make it very difficult to extract significant signals of aerosol effects on monsoon water cycle variability. In

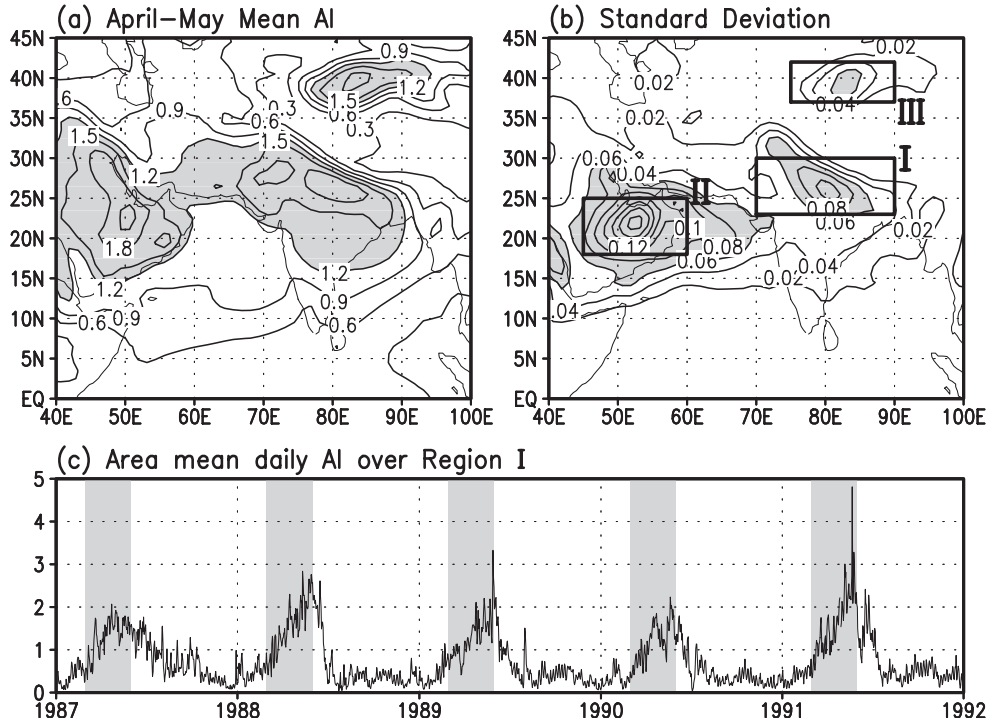

Figure 1 Climatological distribution of absorbing aerosols over the Indian subcontinent and adjacent areas based on the TOMS Aerosol Index (AI) for April-May showing a) the bi-monthly mean distribution, and b) the standard deviation, and c) Area mean daily AI over region I. Key source regions are marked by numbered rectangles in b)

this regard, the aforementioned modeling studies will provide valuable guidance on how and where to look for such signals in observations.

In this article, we show observations in support of the notion that aerosol forcing in late spring and early summer may induce Asian monsoon anomalies, and discuss how the radiative imbalance induced by absorbing aerosols may be instrumental in triggering dynamical feedback in the monsoon water cycle. For aerosol observations, we will use the Total Ozone Mapping Spectrometer (TOMS) Aerosol Index (AI). The TOMS AI is a measure of the wavelength-dependent change in Rayleigh-scattered radiance from aerosol absorption and is especially suitable for detecting the presence of absorbing aerosols above high reflecting surfaces, such as desert, and snow/ice over land, where MODIS has difficulties (Hsu et al. 1999). The AI data set is the only long-term continuous daily global record for absorbing aerosols (mainly black carbon and dust). It starts in November 1978 and, with the exception of a data gap from May 1993 to August 1996, runs to the present.

Figure 1a shows the April-May climatological (1979-1992) distribution of AI over the greater Indian monsoon region. Three major source regions can be identified: I) The Ganges Plain over northern India (marked by the rectangular box in the figure), II) Saudi Arabia and the Iran/Afghanistan/Pakistan deserts, and III) Western Asia over the Taklamakan desert. The interannual variability of the aerosol loading (Fig. 1b) is found to be about 10-15% of the bimonthly mean, and is strongest over the Middle East region, but also significant over region I and III. Aerosol radiative forcing from these regions may alter the large-scale thermal contrast in the troposphere and between the land surface and the adjacent oceans. In addition, dusts from Regions II may be transported to Region I, and mix with the black carbon produced from local emissions, further altering the atmospheric heat source and sink distribution. Since aerosol emission and transport is dependent on the soil types, the winds and the rainfall, the total dust loading in all three source regions undergo multi-scale variability associated with the monsoon climate system. The AI index in Region I (Fig. 1c) shows the strong seasonality of the aerosol loading, with increasing concentration in boreal spring (March-April-May), maximum near the latter part of May, and reducing concentration in fall and winter. The yearly variability as well as the intraseasonal variability of aerosol amount is quite obvious. Some years, the removal of aerosol from the atmosphere is very rapid, reaching minimum level days after the Indian monsoon onset in early-to-mid June, e.g. 1988. Other years, the aerosol removal is much slower, e.g. 1987. The year 1987 (1988) is well known as a weak (strong) monsoon year. The real question here is whether aerosol is a contributing factor to the monsoon anomaly.

The latitude-time cross sections of composite of four years (1980, 1985, 1988, 1991) of high AI anomaly (Fig. 2a, page 17), shows a slow build up of the aerosol loading up to May, and the rapid removal in June-July-August during the monsoon season. There appears to be a northward migration of rainfall anomaly from equatorial oceanic region to the monsoon land region, and an intensification of the monsoon rainfall (15°N–25°N) in June-July (Fig.2b), following the aerosol build-up in May. Over the Indian subcontinent, the rainfall season seems to have advanced with more rain appearing in the early part, and less rain in the latter part of the season. Fig. 2c shows that the rainfall increase in June-July is pan-India, with most pronounced signal over the Western Ghats, and the land region around the Bay of Bengal. The strengthened Indian monsoon is evident in the anomalous low level westerlies over the Indian subcontinent. Over East Asia, a strong anticyclonic anomaly is found, suggesting an intensification, and a westward shift of the Western Subtropical High. As a result, the Mei-yu rainbelt is pushed north of the Yangtze, and eastward over Japan, giving rise to the characteristic north-south dipole rainfall anomaly over East Asia (Lau et al. 2000). The aforementioned results suggest that the large-scale dynamical structure of the entire Asian monsoon system may have been modified by the aerosol forcing.

How can absorbing aerosols over Asia continent trigger a large-scale dynamical monsoon response? We recall that the net radiative effect of aerosols on the atmosphere and the surface depends not only on the aerosol type but also on the albedo and the temperature of the underlying surface. Fig. 3 shows the radiative balance at the top of the atmosphere and at the earth's surface for an amount of desert dust with optical thickness equal to unity over land (albedo = 0.35), and over ocean (albedo = 0.03). The spectral dust properties used in the calculations are based upon values reported in OPAC (Optical Properties of Aerosols and Clouds) for 0.5 μm dust particles (Hess et al. 1998), in which the corresponding equivalent broadband single scattering albedo is approximately 0.92. The calculation is conducted using a climatological atmospheric temperature and moisture sounding over land and ocean, respectively. The net aerosol forcing is defined as the difference in total radiation flux between a pristine atmosphere and a dusty atmosphere.

When we look at aerosol forcing over land and ocean surfaces for these conditions we find that the total atmosphere-land system warms by 8 Wm^{-2}, while the total atmosphere-ocean system cools by 78 Wm^{-2}. For the atmospheric component itself (surface minus top-of-atmosphere), our calculations show that the atmosphere over the ocean is heated by 97 Wm^{-2}, while over land the atmospheric heating is significantly stronger at 115 Wm^{-2}. This is due to enhanced dust absorption associated with the multiple reflections of solar radiation between the high albedo land surface and the dust layer. The overall result is that the cooling over land surfaces is usually much smaller than that over ocean surfaces. It is possible, over elevated land such as snow covered surfaces of the

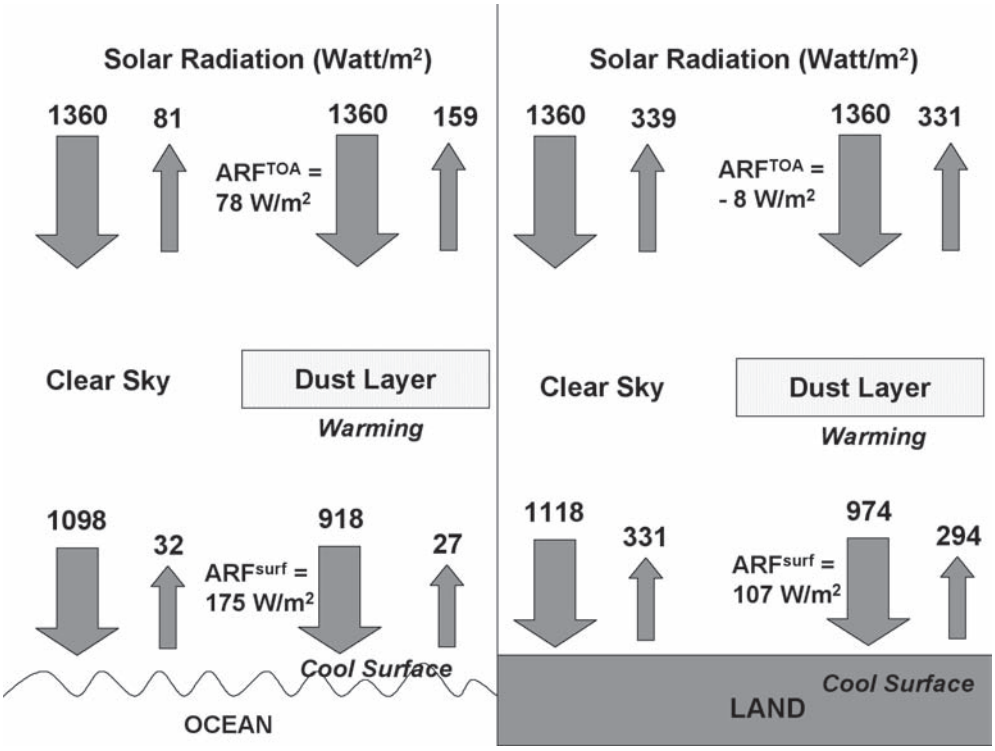

Figure 3 Schematic showing the aerosol radiative forcing induced a dust layer of unit optical thickness over a dark ocean (left panel) and over a bright land surface (right panel).

Himalayas, that the aerosol forcing, combined with the sensible heat flux from the dust layer to the surface, may reverse the sign of the net aerosol forcing at the surface and cause the land surface to warm. The reversal of the meridional gradient in upper tropospheric temperature between the Tibetan Plateau and the oceanic region to the south is known to have a strong control on the timing of the onset and evolution of the Asian monsoon (Li and Yanai, 1996). Therefore, it is possible that, the aerosol-induced differential heating in late spring, amplified through the "elevated heat pump" effect may cause an early reversal of such a temperature gradient subsequently leading to an advance of the monsoon season, and an intensification via induced feedback processes associated with the monsoon water cycle.

Reference

Hess, M, P. Koepke, and I. Schult , 1998: Optical Properties of Aerosols and clouds: The software package OPAC, *Bull. Am. Met. Soc.*, **79**, 831-844.

Hsu, N.C., J. R. Herman, , J. F. Gleason, , O. Torres, , and C. J. Seftor, 1999: Satellite detection of smoke aerosols over a snow/ice surface by TOMS. *Geophys. Res. Lett.*, **26**, 1165-1168.

Lau, K. M., K. M. Kim, and S. Yang, 2000: Dynamical and Boundary Forcing Characteristics of regional components of the Asian summer monsoon. *J. Climate,* **13,** 2461-2482.

Lau, K. M., M. K. Kim and K. M. Kim, 2005: Asian monsoon anomalies induced by aerosol direct effects. Nature, submitted.

Li, C, and M. Yanai, 1996: The onset and interannual variability of the Asian summer monsoon in relation to land-sea thermal contrast. *J. Climate* **9**, 358-375.

Menon, S., J. Hansen, L. Nazarenko, and Y. Luo (2002), Climate effects of black carbon aerosols in China and India, *Science,* **297**, 2250-2253.

Ramanathan V., C. Chung, D. Kim, T. Betge, L. Buja, J. T. Kiehl, W. M. Washington, Q. Fu, D. R. Sikka, and M. Wild, 2005: Atmospheric brown clouds: impacts on South Asian climate and hydrological cycle. *Proc. Natl. Acad. Sci.,* **102**, 5326-5333.www.pnas.org/cgi/doi/10.1073/pnas.0500656102.

Stanhill, G., and S. Cohen, 2001: Global dimming, a review of the evidence for a widespread and significant reduction in global radiation with a discussion of its probable causes and possible agricultural consequences. *Agric. For. Meteorol.,* **107,** 255-278.

From Lau et al (page 7) Observational evidenc eof effects of absorbing aerosols on season-to-interanuula anomalies of the Asian Monsoon

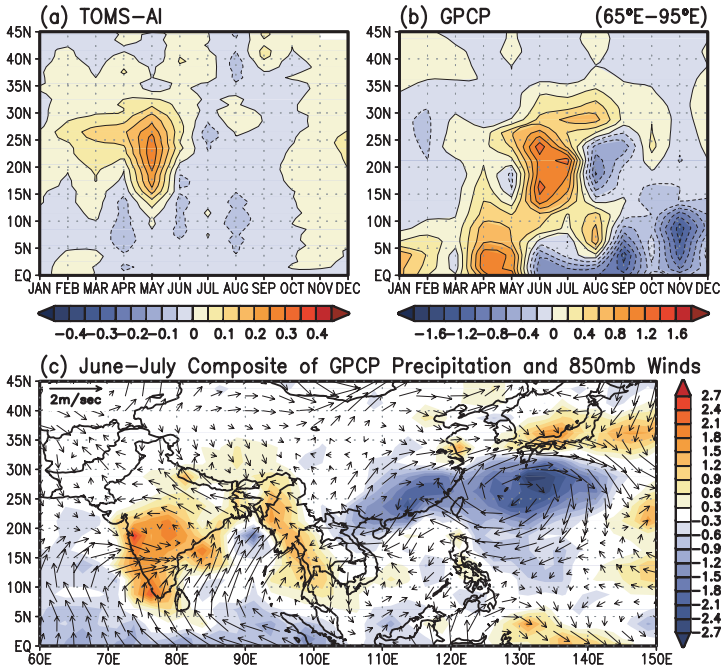

Figure 2 Time-latitude cross-sections showing composite seasonal evolution during year of high AI of a) the AI anomalies, and b) the observed rainfall anomalies, and c) composite of rainfall and 850 hPa wind pattern during years of high AI anomalies.